Synthesis of molybdates Zn1-xCoxMoO4 ($0 \leq x \leq 1$), by decomposition of the precursors developed by the glycine-nitrate process (GNP), and their characterization

Hind Lakhlifi, Youssef El Jabbar, Rachida El Ouatib, Lahcen Er-Rakho, Bernard Durand, Sophie Guillemet-Fritsch

Synthesis of molybdates $Zn_{1-x}Co_xMoO_4$ ($0 \leq x \leq 1$), by decomposition of the precursors developed by the glycine-nitrate process (GNP), and their characterization

Hind Lakhlifi [a], Youssef El Jabbar [a], Rachida El Ouatib [a], Lahcen. Er-Rakho [a], Bernard Durand [b], Sophie Guillemet-Fritsch [b]

[a] Laboratoire de Physico-chimie des Matériaux Inorganiques, Faculté des sciences Aïn chock, Université Hassan II, Bb. 5366 Mâarif, Casablanca, Morocco.

[b] Institut Carnot CIRIMAT, CNRS Université de Toulouse, 118 route de Narbonne, 31062 Toulouse Cedex 9, France.

Abstract:

Nanocrystals of zinc-cobalt molybdate ($Zn_{1-x}Co_xMoO_4$) were prepared by the glycine-nitrate process (GNP) route with a glycine/nitrate ratio of 2:3 and compared to the solid state synthesis. The obtained powders were characterized by thermal analysis (TGA-TDA), X-ray powder diffraction (XRD), Fourier transform infrared spectroscopy (FTIR) and Raman spectroscopy. The morphology was examined by scanning electron microscopy (SEM) and Brunauer–Emmett–Teller (BET). The particle size was determined by transmission electron microscopies (TEM). UV-Visible spectroscopy and CIE L*a*b* colorimetric parameters have been used for the colour characterisation and measurement. The compounds obtained present two single-phased domains regardless of the synthesis method. The first domain of blue colour corresponding to a level of cobalt x such as: $0 \leq x \leq 0.3$, isostructural with α-$ZnMoO_4$ of triclinic symmetry and the second domain of green colour, for cobalt x levels such as: $0.45 \leq x \leq 1$ isostructural with α-$CoMoO_4$ of monoclinic structure. The $Zn_{0.7}Co_{0.3}MoO_4$ powders obtained at 700°C by GNP route and synthesized in acidic environment were formed of particles of quasi-spherical morphology, with average size of crystallites estimated between 80 - 140 nm.

Keywords: Molybdates; XRD; Synthesis; Morphology; Glycine-nitrate process; Solid state.

1. Introduction

The molybdates of bivalent elements known by the formula $AMoO_4$ (A = bivalent element) have been widely studied in recent years because of their remarkable optical properties [1,2]. These oxides are thermochromic and piezochromic materials that present phase transitions associated with strong changes in colour and the doping by various chemical elements can be modify temperatures and pressure transitions [3]. Metal molybdates with monoclinic/triclinic systems have various potential uses, such as for photoluminescence, semiconductor lasers, magnetism, lithium–ion batteries, microwave applications, catalysis, photoelectric devices, photonic crystals, and chemical reactors [4–7].

The present paper focuses on the synthesis of zinc molybdate substituted with cobalt. In this structure, the zinc atoms are bound to six oxygen atoms, forming distorted octahedral clusters $[ZnO_6]$[8]. Molybdenum atoms are associated with four oxygen atoms, resulting in tetrahedral clusters $[MoO_4]$, while the Zn^{2+} ions occupy two sites of different symmetry: octahedral and bipyramidal triangular bases [9]. The presence of the cobalt ions in these sites induces differentiable colours resulting from the d-d electron transitions [10]. Several synthesis methods have been used to synthesize the molybdate $AMoO_4$, such as the solvothermal method [11], co-precipitation [12,13], the Pechini method [14], the molten salt method [15], and the sol–gel route [16]. This work presents a synthesis of cobalt-zinc molybdate using the Glycine–Nitrate-Process (GNP) route based on exothermic redox reactions. Compared to the conventional solid state method, this method creates more reactive precursors that lead to powders with a high specific surface area at low annealing temperatures.

2. Methods and materials

The reagents used to develop the precursors of the molybdate $Zn_{1-x}Co_xMoO_4$ are zinc nitrate ($Zn(NO_3)_2$, $6H_2O$) (Aldrich, 98%), cobalt nitrate ($Co(NO_3)_2$, $6H_2O$) (Aldrich, 98%), and ammonium heptamolybdate ($(NH_4)_6Mo_7O_{24}$, $4H_2O$) (Acros, 99%). These reagents were mixed in stoichiometric proportions. Glycine was then introduced in a molar ratio of glycine/nitrates of 2:3. After evaporation at 110°C, the precursors obtained were pre-calcined at 300°C for 12 hours. The resulting black powder was heat treated for 2 hours at a determined temperature. Depending on the amount of cobalt ($0 \leq x \leq 1$), different colors were obtained after grinding. The synthesized powders were characterized using an x-ray diffractometer (Bruker D8 Advance equipped with a detector LynxEye, CuKα, λ=1.5406 Å), and the infrared spectra were taken using an FTIR spectrometer (IR Affinity-1S Shimadzu).

The Raman spectra were recorded with a LabRAM HR 800 (Horiba Jobin-Yvon) spectrometer, and UV–vis measurements were taken with a Perkin Elmer Lambda 35 spectrophotometer. The morphology of the powders was examined using scanning electronic microscopy (JEOL JSM 6400), and the measurements of specific surface areas were determined using the BET method (Micrometrics Flowsorb II 2300). The colour parameters (L*, a*, b*) were measured using the CIE Lab system colorimeter (CR-400/410, KONICA MINOLTA).

3. Results and discussion

3.1. Thermal decomposition

Thermal analysis (TGA/DTA) was performed to monitor the thermal decomposition process of the precursors synthesized by GNP route, and to estimate the calcination temperature (Fig. 1(a) and (b)). Fig 1(a) presents the thermal decomposition of the precursor of $Zn_{0.7}Co_{0.3}MoO_4$ which occurred over several steps. An initial weight loss of 9% was observed between 50°C and 150°C, corresponding to the elimination of superficially adsorbed water. Pyrolysis showed a weight loss of 5% in the temperature range of 200–310°C and a more significant loss of 12% at 450°C, which was accompanied by an exothermic peak. For the precursor of the molybdates $Zn_{0.4}Co_{0.6}MoO_4$ (Fig. 1(b)), the loss attributed to the elimination of water was less (3%), and the combustion of organic water occurred in one step, involving a weight loss of 8% accompanied by an exothermic peak at 430°C. Beyond 600°C, no weight loss was observed, indicating that the decomposition was complete and confirming that 700°C was the most appropriate temperature for obtaining pure phases free of organic residue.

Fig. 2(a) and (b) show the thermogravimetric analysis in air of the mixtures of nitrates used for the preparation by the solid-state reactions of the molybdates $Zn_{0.8}Co_{0.2}MoO_4$ and $Zn_{0.4}Co_{0.6}MoO_4$ powders. The observed weight losses were 20% and 36%, respectively. These losses agreed with those calculated for dehydration and the decomposition of nitrates (19% for the compound with x=0.2 and 33% for x=0.6). These transformations are shown by endothermic peaks on the DTA curves. No phenomena were observed above 500°C; thus, decomposition was complete.

3.2. X-ray diffraction characterisation

Figure 3 shows the XRD patterns of powders prepared using the GNP route in an acidic medium (pH=3), treated at 700°C for 2 hours, and ground. As shown in Fig. 4, the following observations were made:

- For $0 \leq x \leq 0.30$, the powder was monophased and isostructural with triclinic α-$ZnMoO_4$ (JCPDS file No. 070-5365).
- For x=0.35 and x=0.40, the powder presents two-phase mixture, one majority isostructural phase with monoclinic α-$CoMoO_4$ (JCPDS file No. 073-1331) and minority phase isostructural with triclinic α-$ZnMoO_4$ (JCPDS file: No. 070-5365) .
- For $0.45 \leq x \leq 1$, the powder was monophased and isostructural with α-$CoMoO_4$.

The diffractograms of the compound $Zn_{0.7}Co_{0.3}MoO_4$ obtained at a basic pH were given in Fig. 5. The XRD peaks have a minimal width at half-height, implying a large average size for crystallites compared to the composition prepared in an acidic medium. An acidic medium accelerates hydrolysis and promotes condensation at the ends of chains, resulting in less dispersed species. A basic environment slows down hydrolysis and promotes condensation in the middle of chains, leading to highly branched (i.e., condensed) species [15]. This hypothesis was verified by the TEM observations of the $Zn_{0.7}Co_{0.3}MoO_4$ synthesized in acid, and basic medium which the TEM micrographs reveal that the average crystallite sizes was between 80-140 nm (Fig. 6 (a)) and 1-5 um (Figure 6 (b)), respectively. This shows the influence of the pH parameter on the morphology of powders developed by this route.

For the molybdates $Zn_{1-x}Co_xMoO_4$ prepared using solid-state reactions at 700°C, the XRD patterns (Fig. 7) show the same phase composition as those for molybdates synthesized using the GNP route; that is, one isostructural phase with α-$ZnMoO_4$ for $x \leq 0.3$, one isostructural phase with α-$CoMoO_4$ for $x \geq 0.45$, and a mixture of both phases for the intermediate compositions. The ball and stick representation of the crystal structure is given in Fig. 8.

3.3. Infrared characterization

In order to confirm the results of X-ray diffraction, spectroscopy analyses (FTIR) were carried out on $Zn_{1-x}Co_xMoO_4$ (x=0.3 and x=0.6) powders prepared by GNP method and obtained at 700°C (Fig. 7). As shown in Fig. 9, both samples have similar IR spectra, Regardless to the synthesis method adopted, showing the presence of 956, 930 and 906 cm^{-1} vibration bands corresponding to $(MoO_4)^{2-}$ tetrahedra. The band observed at 866 cm^{-1} corresponds to O-Zn-O bonds [17,18]. The vibration bands at 750 and 798 cm^{-1} are due to the expansion of the Zn-O-Mo bonds [19–21]. Bands at 663 and 418 cm^{-1} can be attributed to O-Mo-O groups [18]. The band at 430 cm^{-1} is specific to the vibrations of the Co-O-Mo bonds [22]. This result confirms the formation of the solid solution $Zn_{1-x}Co_xMoO_4$.

3.4. Raman spectroscopy characterization

Raman analysis was performed on the $Zn_{0.7}Co_{0.3}MoO_4$ and $Zn_{0.4}Co_{0.6}MoO_4$ samples obtained at 700°C by the GNP route (Fig. 10). According to the literature, MoO_n polyhedrons, MoO_4 tetrahedrons and MoO_6 octahedrons give Raman strong bands. Generally, Raman bands corresponding to the symmetrical stretching (υ_1) and asymmetrical stretching (υ_3) modes were observed in the 700-1000 cm^{-1} region, whereas those corresponding to the symmetrical modes (υ_2) and asymmetrical modes (υ_4) were observed in the 50-520 cm^{-1} region [23-25]. For the $Zn_{0.7}Co_{0.3}MoO_4$ composition, the most intense Raman vibrations were observed at 955 and 933 cm^{-1} , they correspond to the symmetrical stretching modes (υ_1) of the MoO_4 tetrahedron [26]. The bands at 874, 850, 831 and 809 cm^{-1} correspond to the stretching vibration antisymmetrical modes (υ3). Those located at 395, 360 and 328 cm^{-1}correspond, respectively, to anti-symmetrical, symmetrical υ4 (Bg) and bending modes υ2 (Ag). The free rotation mode was observed at 276 cm^{-1} [26]. For the $Zn_{0.4}Co_{0.6}MoO_4$ composition, the Raman bands at 912 and 882 cm^{-1} are associated to the symmetrical stretching mode of the Mo-O bonds. Those located at 834 and 793 cm^{-1} correspond to asymmetric oxygen stretching modes in the O-Mo-O bonds. The bands observed at 360 and 322 cm^{-1} were attributed to the Mo-O-Co stretching vibrations [27–31]. These results were consistent with those obtained by diffraction analysis techniques X-rays and infrared spectroscopy (FTIR).

3.5. Microstructural characterization

The SEM images for $Zn_{0.7}Co_{0.3}MoO_4$ prepared by GNP route show a powder formed of agglomerated particles of varying morphology (Fig. 11 (a)) and for the $Zn_{0.4}Co_{0.6}MoO_4$ (Fig. 11 (b)) an advanced pre-sintering state which can be attributed to the high cobalt rate. While the powders prepared by solid state reactions consisted by agglomerates of grains as revealed in Fig. 12 (a) and (b). The TEM micrograph for $Zn_{0.7}Co_{0.3}MoO_4$ powder prepared by GNP route (Fig. 13 (a)) reveal elementary grains of more or less spherical shape with average size estimated between 80 and 140 nm. While that prepared by solid state reaction (Fig. 13 (b)) show agglomerated particles with average size of a few micrometers.

3.6. Colours analysis

The colour parameters (L*, a*, b*) of the powders obtained by GNP method and by solid state reactions were measured in the CIE Lab system using a CR-400/410 colorimeter. The evolution of these parameters as a function of the x composition and the pH was given in Fig. 14 (a)-(b) and Fig. 15 (a)-(b) for the compounds obtained by the GNP route and those obtained by solid state reactions, respectively. The component (-b*) characterizing the blue

colour, has a maximum for compositions $0.2 \leq x \leq 0.3$ regardless of the method of synthesis adopted. In the case of samples synthesised by GNP route, the evolution of colour parameters shows that the blue colour appears to develop more for the composition x=0.25 in the basic medium. It seems that the degree of blueness for the samples prepared by solid state increase with annealing temperature.

The origin of the colour difference between $Zn_{0.7}Co_{0.3}MoO_4$ compound noted φ_T and $Zn_{0.4}Co_{0.6}MoO_4$ compound noted φ_M was studied UV-visible spectroscopy (Fig. 16). Whatever the used synthesis method, the spectrum of the triclinical molybdate $Zn_{0.7}Co_{0.3}MoO_4$ (φ_T) shows a single wide and intense absorption band covering wavelengths ranging from 390 to 520 nm and centered at 460 nm which confirms the blue coloration of this molybdate. This band may correspond to the charge transfer between the valence band formed by oxygen-solid atomic orbitals ($2p^6$) and the conduction band formed by empty atomic orbitals of molybdenum and/or cobalt. However, it is known that molybdenum VI is more easily reducible than cobalt II [32], so it is very probably a charge transfer $O^{2-} \rightarrow Mo^{6+}$ ($2p^6 \rightarrow 4d^0$). The energy levels of Zn empty orbitals are too high to be involved in this charge transfer [33-35]. The monoclinical molybdate $Zn_{0.4}Co_{0.6}MoO_4$ (φ_M) spectrum shows two absorption bands at 500 and 540 nm characteristics of the green colour. These bands of low-energy can be attributed to intra-atomic d-d transitions related to Co^{2+} ions in octahedral symmetry [33].

4. Conclusion

The molybdates $Zn_{1-x}Co_xMoO_4$ were synthesized by GNP route and solid state reactions. The X-ray analysis reveals that the compounds obtained at 700°C present two single-phased domains regardless of the synthesis method:

- A first domain of blue colour corresponding to a level of cobalt x such as: $0 \leq x \leq 0.3$, isotype to α-$ZnMoO_4$ of triclinical symmetry.
- A second domain of green colour, for cobalt x levels such as: $0.45 \leq x \leq 1$ isotype to α $CoMoO_4$ of monoclinical structure.

The study by infrared and Raman spectroscopy of the compositions x=0.3 and x=0.6 prepared by the GNP route corroborates the formation of the solid solutions $Zn_{1-x}Co_xMoO_4$.

The UV-Visible absorption spectroscopy study confirms that the origin of blue colour (x=0.3) depends on a charge transfer $O^{2-} \rightarrow Mo^{6+}$. While the green colour (x=0.6) is due to intra - atomic d-d transitions related to Co^{2+} ions in octahedral symmetry.

The morphology examined by SEM and TEM analysis shows that the $Zn_{0.7}Co_{0.3}MoO_4$ powder prepared by GNP route is formed of particles of quasi-spherical morphology, with an average size of crystallites estimated between 80 - 140 nm, in acidic environment.

The colorimetric parameters measurement show the blue colour is highest for composition x=0.25 in cobalt regardless of the method of synthesis adopted.

References

[1] V.M. Anandakumar, M.A. Khadar, Synthesis, characterization and optical properties of nanocrystalline lead molybdate, Phys. Status Solidi A. 205 (2008) 2666–2672. https://doi.org/https://doi.org/10.1002/pssa.200723444.

[2] A.M. Huerta-Flores, I. Juárez-Ramírez, L.M. Torres-Martínez, J.E. Carrera-Crespo, T. Gómez-Bustamante, O. Sarabia-Ramos, Synthesis of $AMoO_4$ (A=Ca, Sr, Ba) photocatalysts and their potential application for hydrogen evolution and the degradation of tetracycline in water, J. Photochem. Photobiol. Chem. 356 (2018) 29–37. https://doi.org/10.1016/j.jphotochem.2017.12.029.

[3] M. Maczka, A.G. Souza Filho, W. Paraguassu, P.T.C. Freire, J. Mendes Filho, J. Hanuza, Pressure-induced structural phase transitions and amorphization in selected molybdates and tungstates, Prog. Mater. Sci. 57 (2012) 1335–1381. https://doi.org/10.1016/j.pmatsci.2012.01.001.

[4] B. Saravanakumar, G. Ravi, R. Yuvakkumar, V. Ganesh, R.K. Guduru, Synthesis of polyoxometalates, copper molybdate ($Cu_3Mo_2O_9$) nanopowders, for energy storage applications, Mater. Sci. Semicond. Process. 93 (2019) 164–172. https://doi.org/10.1016/j.mssp.2019.01.002.

[5] V.D. Araújo, R.L. Tranquilin, F.V. Motta, C.A. Paskocimas, M.I.B. Bernardi, L.S. Cavalcante, J. Andres, E. Longo, M.R.D. Bomio, Effect of polyvinyl alcohol on the shape, photoluminescence and photocatalytic properties of $PbMoO_4$ microcrystals, Mater. Sci. Semicond. Process. 26 (2014) 425–430. https://doi.org/10.1016/j.mssp.2014.05.027.

[6] K.V. Raun, L.F. Lundegaard, J. Chevallier, P. Beato, C.C. Appel, K. Nielsen, M. Thorhauge, A.D. Jensen, M. Høj, Deactivation behavior of an iron-molybdate catalyst during selective oxidation of methanol to formaldehyde, Catal. Sci. Technol. 8 (2018) 4626–4637. https://doi.org/10.1039/C8CY01109E.

[7] Q. Li, X. Zeng, S. Yang, X. Liao, Microwave Synthesis and Photoluminescence Properties of 3 $CaMoO_4$: $Eu^{3+}_{0,1}$ Nanocomposites, 7 (2017) 99–104. https://doi.org/https://doi.org/10.4236/ojcm.2017.72006.

[8] L.S. Cavalcante, J.C. Sczancoski, M. Siu Li, E. Longo, J.A. Varela, β-$ZnMoO_4$ microcrystals synthesized by the surfactant-assisted hydrothermal method: Growth process and photoluminescence properties, Colloids Surf. Physicochem. Eng. Asp. 396 (2012) 346–351. https://doi.org/10.1016/j.colsurfa.2011.12.021.

[9] L. Robertson, M. Duttine, M. Gaudon, A. Demourgues, Cobalt-zinc Molybdates as New Blue Pigments Involving Co^{2+} in Distorted Trigonal Bipyramids and Octahedra, Chem. Mater. 23 (2011) 2419–2427. https://doi.org/10.1021/cm200795p.

[10] S.F. Matar, A. Largeteau, G. Demazeau, $AMoO_4$ (A=Mg, Ni) molybdates: Phase stabilities, electronic structures and chemical bonding properties from first principles, Solid State Sci. 12 (2010) 1779–1785. https://doi.org/10.1016/j.solidstatesciences.2010.07.030.

[11] Y. Keereeta, T. Thongtem, S. Thongtem, Effect of medium solvent ratios on morphologies and optical properties of α-$ZnMoO_4$, β-$ZnMoO_4$ and $ZnMoO_4 \cdot 0.8H_2O$ crystals synthesized by microwave-hydrothermal/solvothermal method, Superlattices Microstruct. 69 (2014) 253–264. https://doi.org/10.1016/j.spmi.2014.02.011.

[12] M.-C. Liu, L.-B. Kong, C. Lu, X.-M. Li, Y.-C. Luo, L. Kang, Facile fabrication of $CoMoO_4$ nanorods as electrode material for electrochemical capacitors, Mater. Lett. 94 (2013) 197–200. https://doi.org/10.1016/j.matlet.2012.12.057.

[13] M. Ghaed-Amini, M. Bazarganipour, M. Salavati-Niasari, K. Saberyan, Morphology and photoluminescence of $BaMoO_4$ micro- and nano-crystals synthesized by coprecipitation method, Trans. Nonferrous Met. Soc. China. 25 (2015) 3967–3973. https://doi.org/10.1016/S1003-6326(15)64045-6.

[14] Z. Zhao, Z. Sui, X. Wei, J. Zuo, X. Zhang, R. Dai, Z. Zhang, Z. Ding, Structure transformation and remarkable site-distribution modulation of Eu^{3+} ions in $CaMoO_4$:Eu^{3+} nanocrystals under high pressure, CrystEngComm. 17 (2015) 7905–7914. https://doi.org/10.1039/C5CE01580D.

[15] J. Ahmed, M. Ubiadullah, N. Alhokbany, S.M. Alshehri, Synthesis of ultrafine $NiMoO_4$ nano-rods for excellent electro-catalytic performance in hydrogen evolution reactions, Mater. Lett. 257 (2019) 126696. https://doi.org/10.1016/j.matlet.2019.126696.

[16] V. Umapathy, P. Neeraja, A. Manikandan, P. Ramu, Synthesis of $NiMoO_4$ nanoparticles by sol-gel method and their structural, morphological, optical, magnetic and photocatlytic properties, Trans. Nonferrous Met. Soc. China. 27 (2017) 1785–1793. https://doi.org/10.1016/S1003-6326(17)60201-2.

[17] A. Kumar Mishra, Sol-gel based nanoceramic materials, Springer Berlin Heidelberg, New York, NY, 2016. https://doi.org/10.1007/978-3-319-49512-5.

[18] K. Seevakan, A. Manikandan, P. Devendran, A. Baykal, T. Alagesan, Electrochemical and magneto-optical properties of cobalt molybdate nano-catalyst as high-performance supercapacitor, Ceram. Int. 44 (2018) 17735–17742. https://doi.org/10.1016/j.ceramint.2018.06.240.

[19] V. Srirapu, A. Kumar, N. Kumari, P. Srivastava, R.N. Singh, A comparative study of electrocatalytic performance of metal molybdates for the water oxidation, Int. J. Hydrog. Energy. 43 (2018) 16543–16555. https://doi.org/https://doi.org/10.1016/j.ijhydene.2018.07.060.

[20] K. Nakamoto, Infrared and Raman Spectra of Inorganic and Coordination Compounds: Part A: Theory and Applications in Inorganic Chemistry, Sixth Edition, 2009.

[21] B.J. Reddy, P. Vickraman, A.S. Justin, A facile synthesis of novel α-$ZnMoO_4$ microspheres as electrode material for supercapacitor applications, Bull. Mater. Sci. 42 (2019) 52. https://doi.org/https://doi.org/10.1007/s12034-019-1749-9.

[22] H. Lakhlifi, M. Benchikhi, R. El Ouatib, L. Er-Rakho, S. Guillemet, B. Durand, Synthesis and physicochemical characterization of pigments based on molybdenum «ZnO-MoO_3: Co^{2+}», J. Mater. Environ. Sci.-JMES. 6 (2015) 3465–3469.

[23] P. Yadav, E. Sinha, Structural, photophysical and microwave dielectric properties of α-$ZnMoO_4$ phosphor, J. Alloys Compd. 795 (2019) 446–452. https://doi.org/10.1016/j.jallcom.2019.05.019.

[24] J. Fu, J.-L. Meng, M.-J. Wei, H.-Y. Zang, H.-Q. Tan, Y.-H. Wang, H. Miras, Y.-G. Li, Cross-Linked $CoMoO_4$/rGO Nanosheets as Oxygen Reduction Catalyst, Catalysts. 7 (2017) 375. https://doi.org/doi:10.3390/catal7120375.

[25] P.J. Mafa, B. Ntsendwana, B.B. Mamba, A.T. Kuvarega, Visible Light Driven $ZnMoO_4$/$BiFeWO_6$/rGO Z-Scheme Photocatalyst for the Degradation of Anthraquinonic Dye, J. Phys. Chem. C. 123 (2019) 20605–20616. https://doi.org/DOI: 10.1021/acs.jpcc.9b05008.

[26] B. Bakiz, F. Guinneton, J.R. Gavarri, Structural and Temperature-dependent vibrational analyses of the non-centrosymmetric $ZnMoO_4$ molybdate, J Mater Env. Sci. 7 (2016) 3076–3083.

[27] N. Padmanathan, H. Shao, S. Selladurai, C. Glynn, C. O'Dwyer, K.M. Razeeb, Pseudocapacitance of α-$CoMoO_4$ nanoflakes in non-aqueous electrolyte and its bi-functional electro catalytic activity for methanol oxidation, Int. J. Hydrog. Energy. 40 (2015) 16297–16305. https://doi.org/http://dx.doi.org/10.1016/j.ijhydene.2015.09.127.

[28] T. Meng, H. Jia, H. Ye, T. Zeng, X. Yang, H. Wang, Y. Zhang, Facile Preparation of $CoMoO_4$ Nanorods at Macroporous Carbon Hybrid Electrocatalyst for Non-enzymatic Glucose Detection, J. Colloid Interface Sci. (2019). https://doi.org/https://doi.org/10.1016/j.jcis.2019.10.054.

[29] Y. Chen, Y. Wang, X. Shen, R. Cai, H. Yang, K. Xu, A. Yuan, Z. Ji, Cyanide-metal framework derived $CoMoO_4$/Co_3O_4 hollow porous octahedrons as advanced anodes for high performance lithium ion batteries, J. Mater. Chem. A. 6 (2018) 1048–1056. https://doi.org/10.1039/C7TA08868J.

[30] F. Nti, D.A. Anang, J.I. Han, Facilely synthesized $NiMoO_4$/$CoMoO_4$ nanorods as electrode material for high performance supercapacitor, J. Alloys Compd. 742 (2018) 342–350. https://doi.org/https://doi.org/10.1016/j.jallcom.2018.01.289.

[31] L. Fang, F. Wang, T. Zhai, Y. Qiu, M. Lan, K. Huang, Q. Jing, Hierarchical $CoMoO_4$ nanoneedle electrodes for advanced supercapacitors and electrocatalytic oxygen evolution, Electrochimica Acta. 259 (2018) 552–558. https://doi.org/10.1016/j.electacta.2017.11.012.

[32] D.A. Kuznetsov, Z. Chen, P.V. Kumar, A. Tsoukalou, A. Kierzkowska, P.M. Abdala, O.V. Safonova, A. Fedorov, C.R. Müller, Single Site Cobalt Substitution in 2D Molybdenum Carbide (MXene) Enhances Catalytic Activity in the Hydrogen Evolution Reaction, J. Am. Chem. Soc. 141 (2019) 17809–17816. https://doi.org/10.1021/jacs.9b08897.

[33] M. Pirhashemi, A. Habibi-Yangjeh, Facile fabrication of novel ZnO/$CoMoO_4$ nanocomposites: Highly efficient visible-light-responsive photocatalysts in degradations of different contaminants, J. Photochem. Photobiol. Chem. 363 (2018) 31–43. https://doi.org/10.1016/j.jphotochem.2018.05.027.

[34] R.K.S. Costa, S.C. Teles, P.C. de Sousa Filho, A. Dias, K.P.F. Siqueira, Influence of europium doping on the structural phase-transition temperature of β− and α−$CoMoO_4$ polymorphs, Mater. Res. Bull. 118 (2019) 110517. https://doi.org/10.1016/j.materresbull.2019.110517.

[35] V. Jeseentharani, A. Dayalan, K.S. Nagaraja, Co-precipitation synthesis, humidity sensing and photoluminescence properties of nanocrystalline Co^{2+} substituted zinc(II)molybdate ($Zn_{1-x}Co_xMoO_4$; x = 0, 0.3, 0.5, 0.7, 1), Solid State Sci. 67 (2017) 46–58. https://doi.org/10.1016/j.solidstatesciences.2017.02.008.

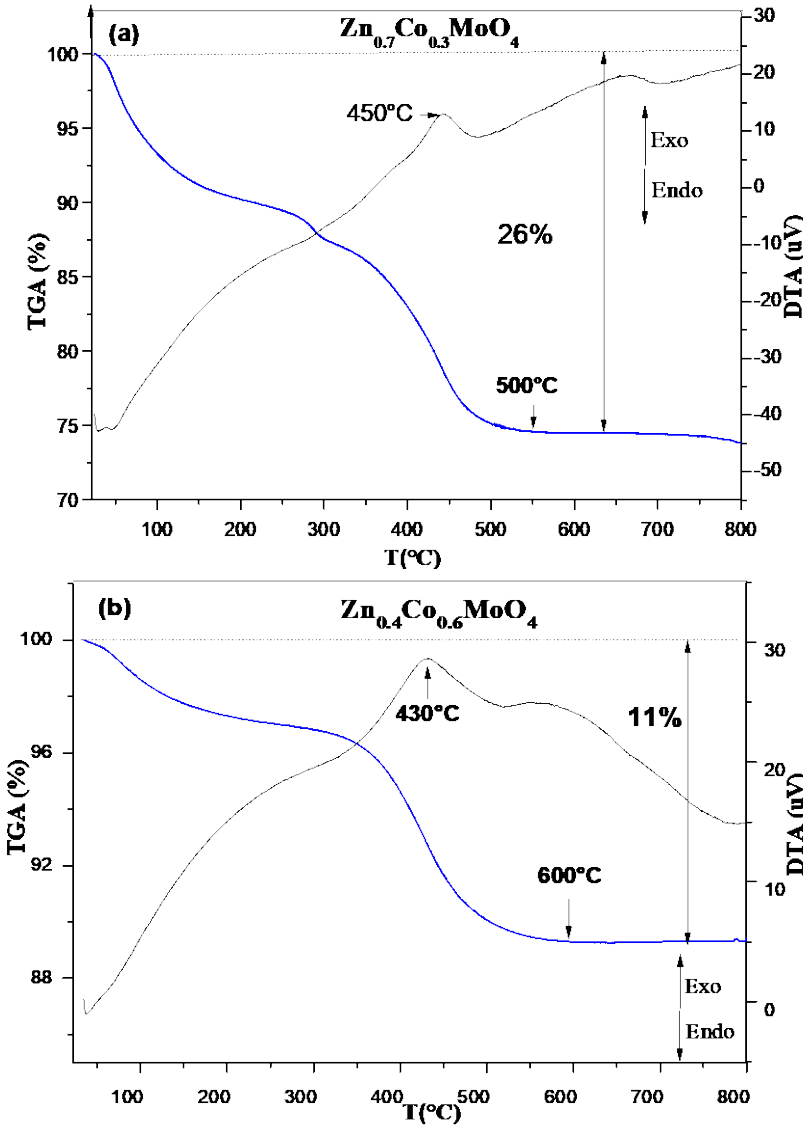

Fig. 1. TGA–DTA curves of (a) the $Zn_{0.7}Co_{0.3}MoO_4$ and (b) the $Zn_{0.4}Co_{0.6}MoO_4$ precursors prepared by GNP route.

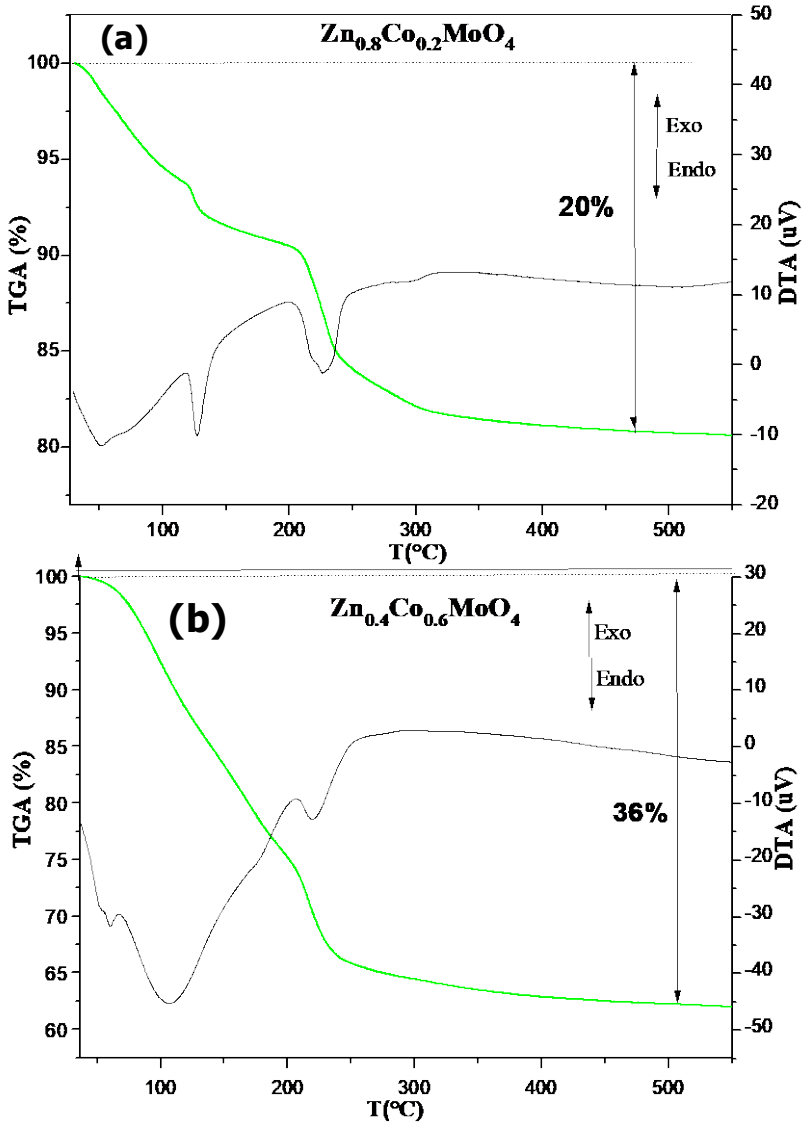

Fig. 2. TGA–DTA curves of (a) the $Zn_{0.8}Co_{0.2}MoO_4$ and (b) the $Zn_{0.4}Co_{0.6}MoO_4$ precursors prepared by solid-state reactions.

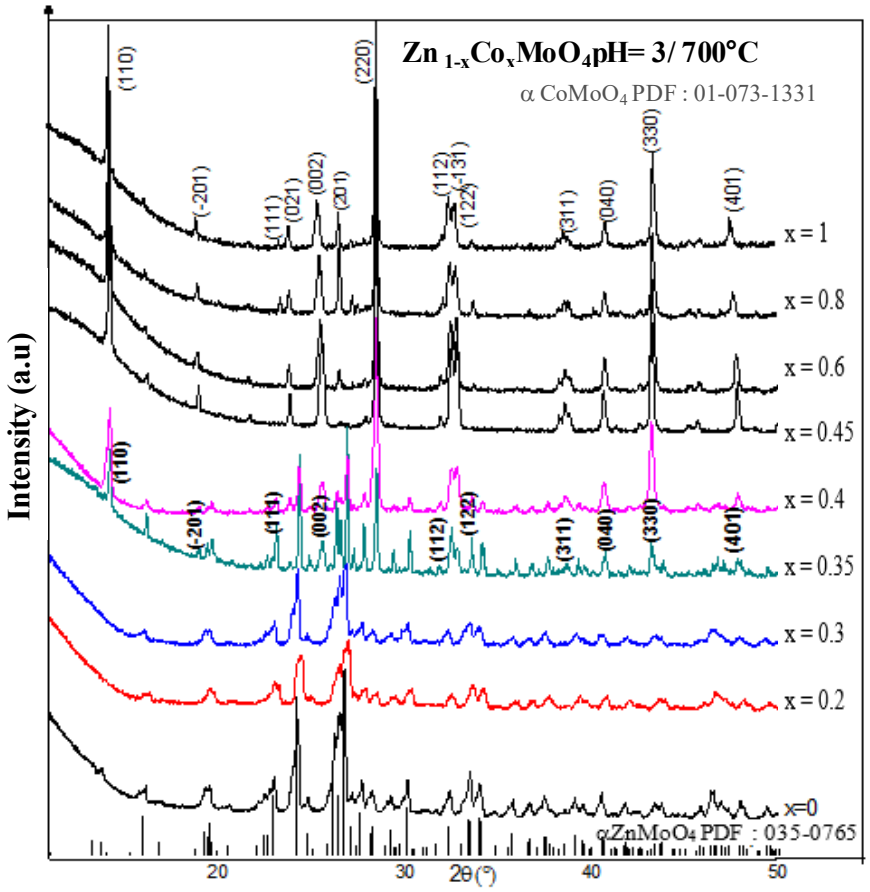

Fig. 3. XRD patterns of $Zn_{1-x}Co_xMoO_4$ $0 \leq x \leq 1$ compounds prepared at 700°C in acid medium.

Fig.4. Structures and phase compositions of $Zn_{1-x}Co_xMoO_4$ compounds.

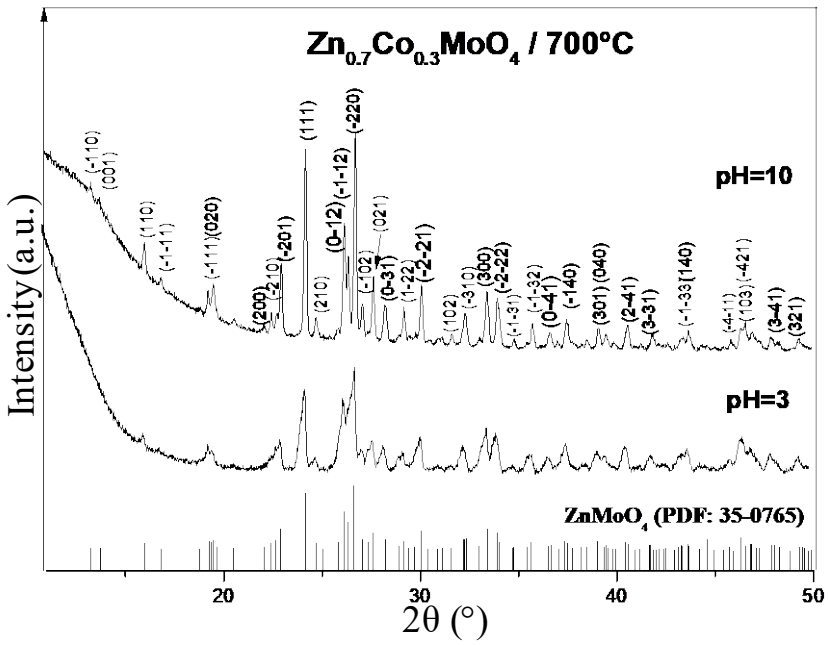

Fig. 5. XRD patterns of $Zn_{0.7}Co_{0.3}MoO_4$ compound synthesized in acid and basic pH.

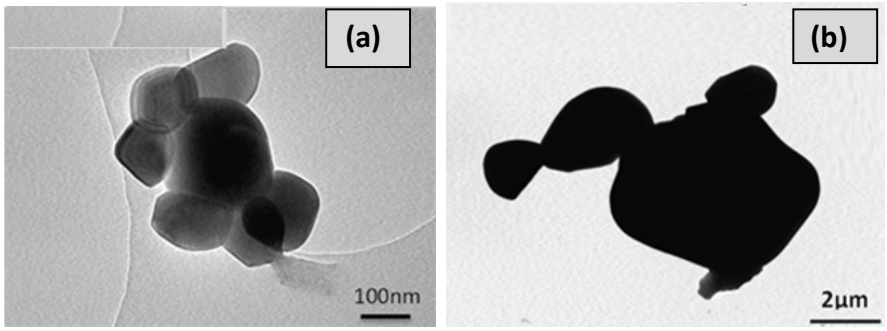

Fig. 6. TEM micrographs of $Zn_{0.7}Co_{0.3}MoO_4$ powders synthesized in acid medium (a) and basic medium and obtained at 700°C for 2h.

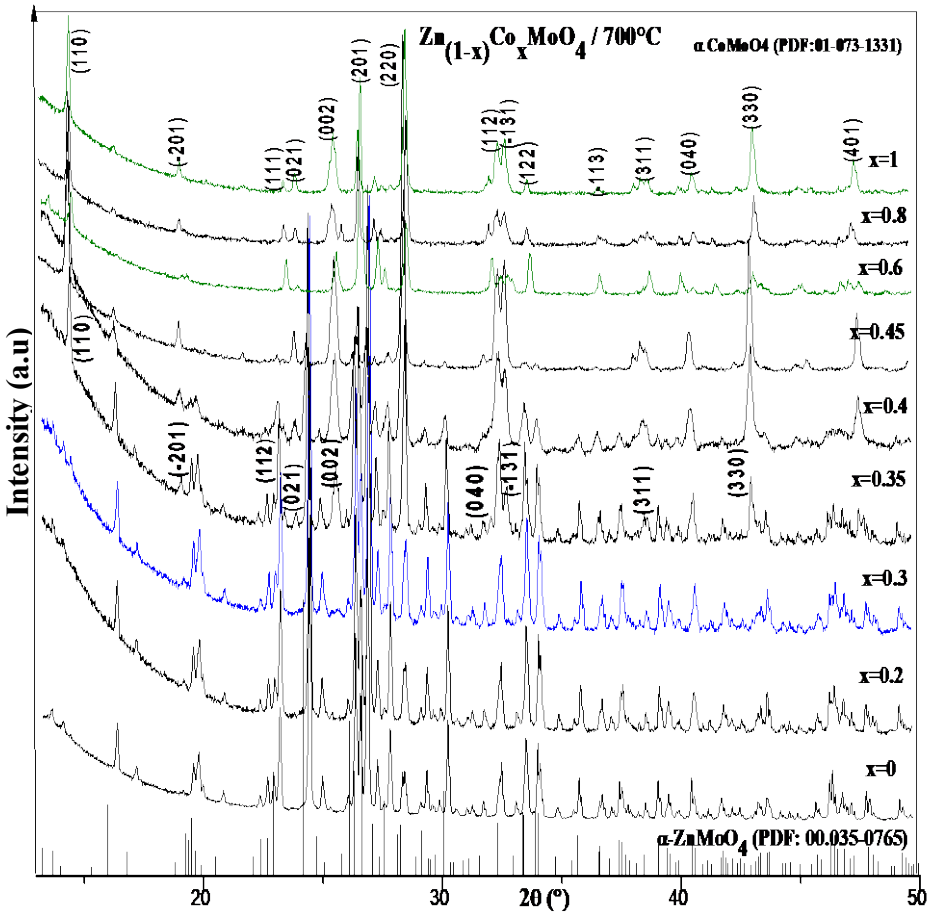

Fig.7. XRD patterns of $Zn_{1-x}Co_xMoO_4$ $0 \leq x \leq 1$ compounds prepared at 700°C by solid state reactions.

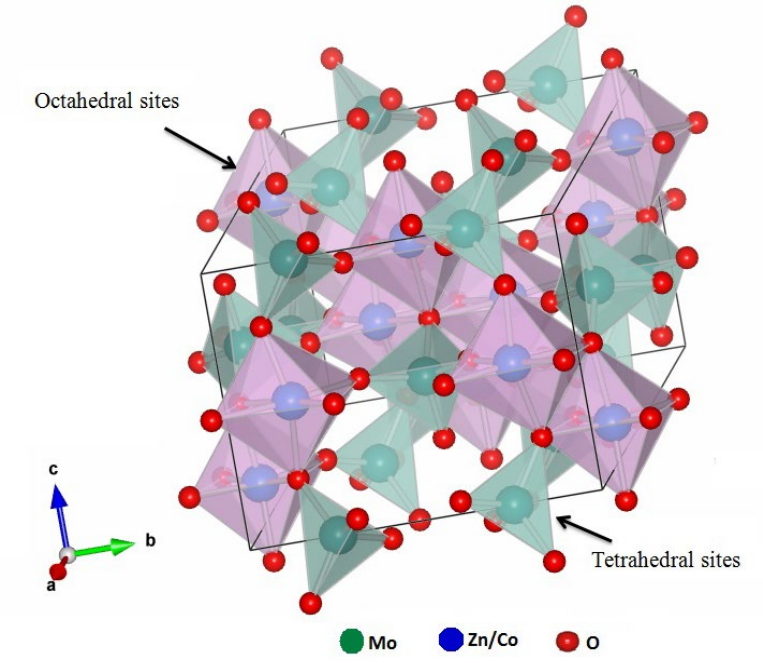

Fig. 8. Ball and stick representation of crystal structure of the $Zn_{1-x}Co_xMoO_4$

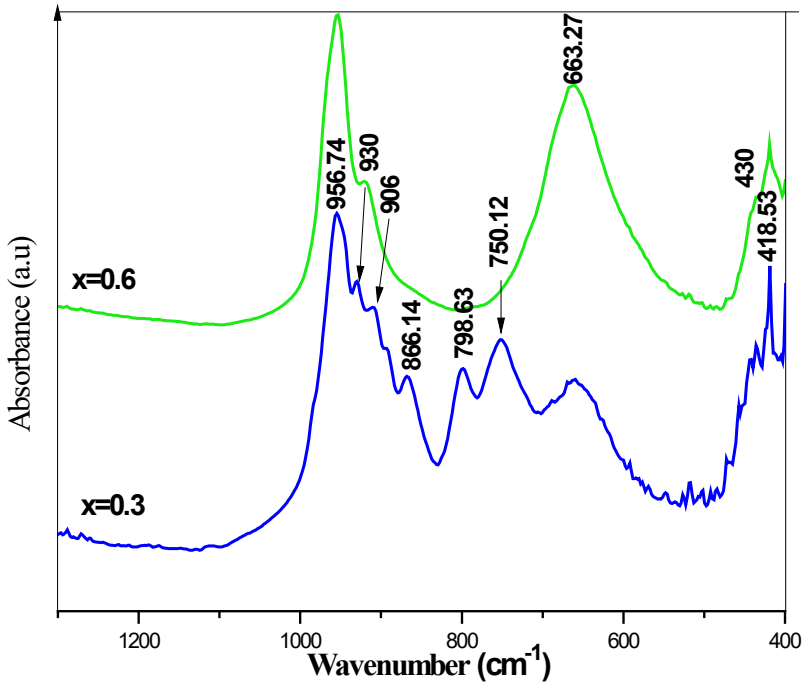

Fig. 9. FT-IR spectra of $Zn_{1-x}Co_xMoO_4$ (x=0.3 and x=0.6) powders obtained at 700°C.

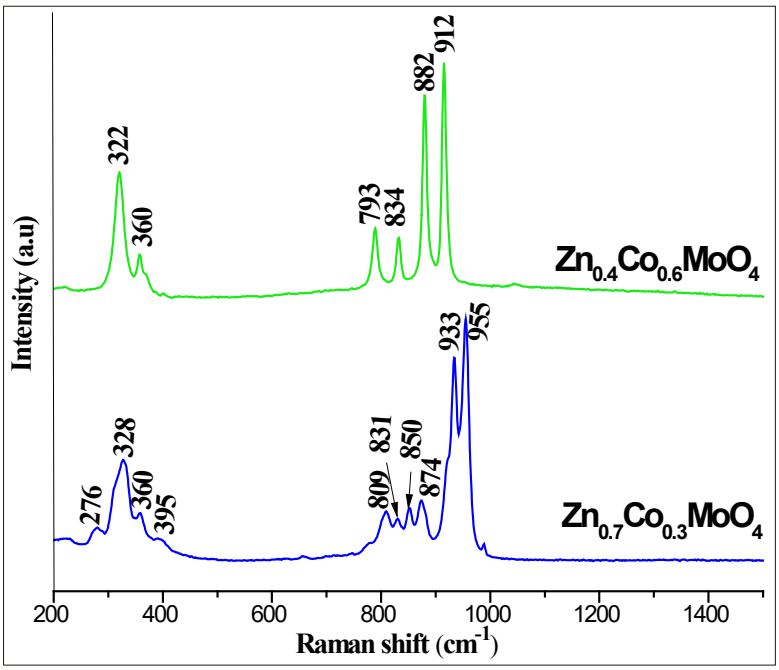

Fig. 10. Raman Spectra of the molybdates $Zn_{0,7}Co_{0,3}MoO_4$ and $Zn_{0,4}Co_{0,6}MoO_4$ prepared by the GNP route

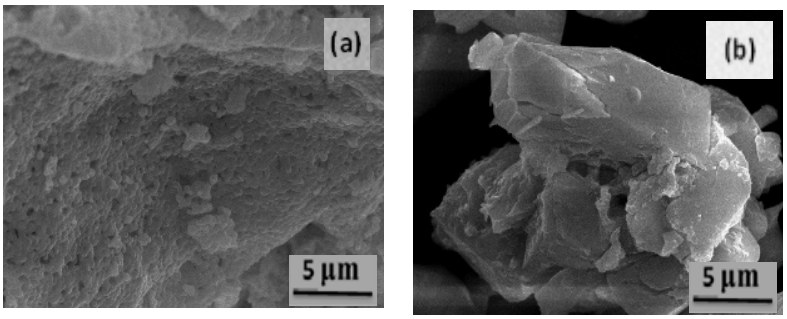

Fig. 11. SEM micrographs of the compositions x=0.3(a) and x=0.6 (b) prepared by GNP route.

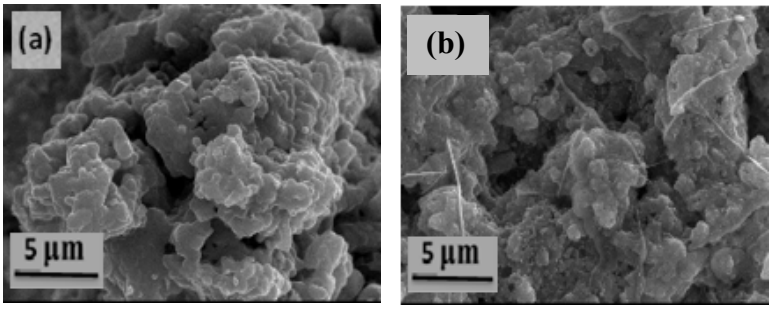

Fig. 12. SEM micrographs of the compositions x=0.3(a) and x=0.6 (b) prepared by solid state reactions.

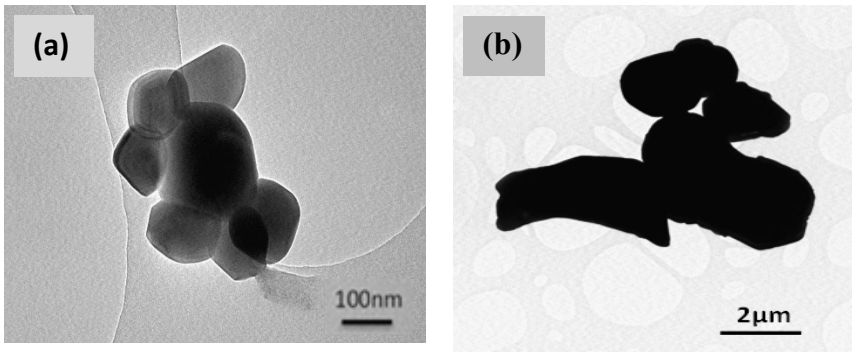

Fig.13. TEM micrographs of $Zn_{0.7}Co_{0.3}MoO_4$ prepared by (a) GNP route and (b) solid state reactions.

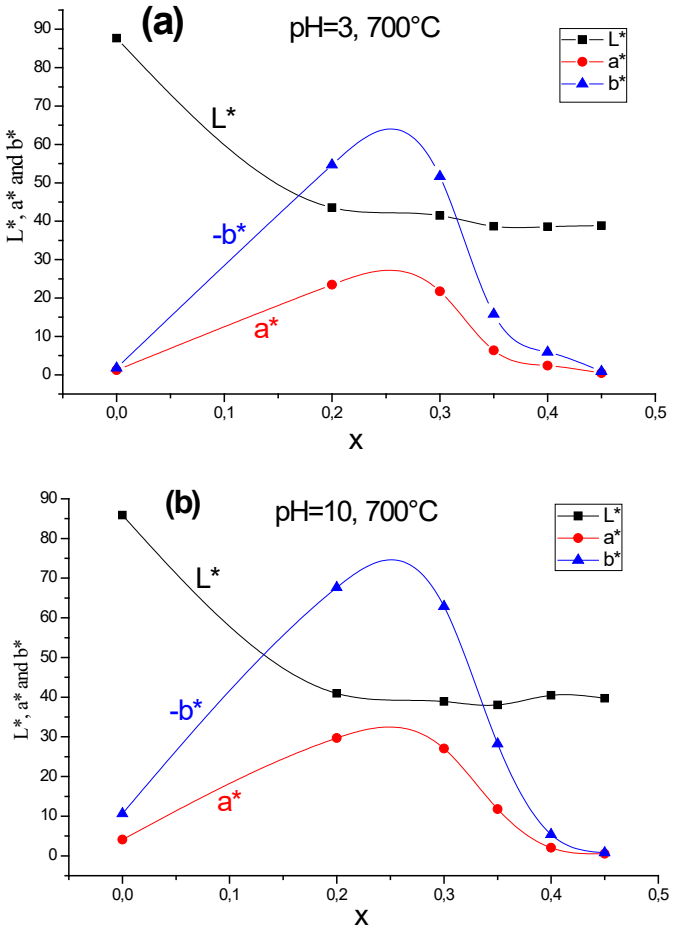

Fig. 14. Evolution of the colour parameters of $Zn_{1-x}Co_xMoO_4$ powders with $0 \leq x \leq 0.45$ obtained by GNP route at pH=3 (a) and pH=10 (b)

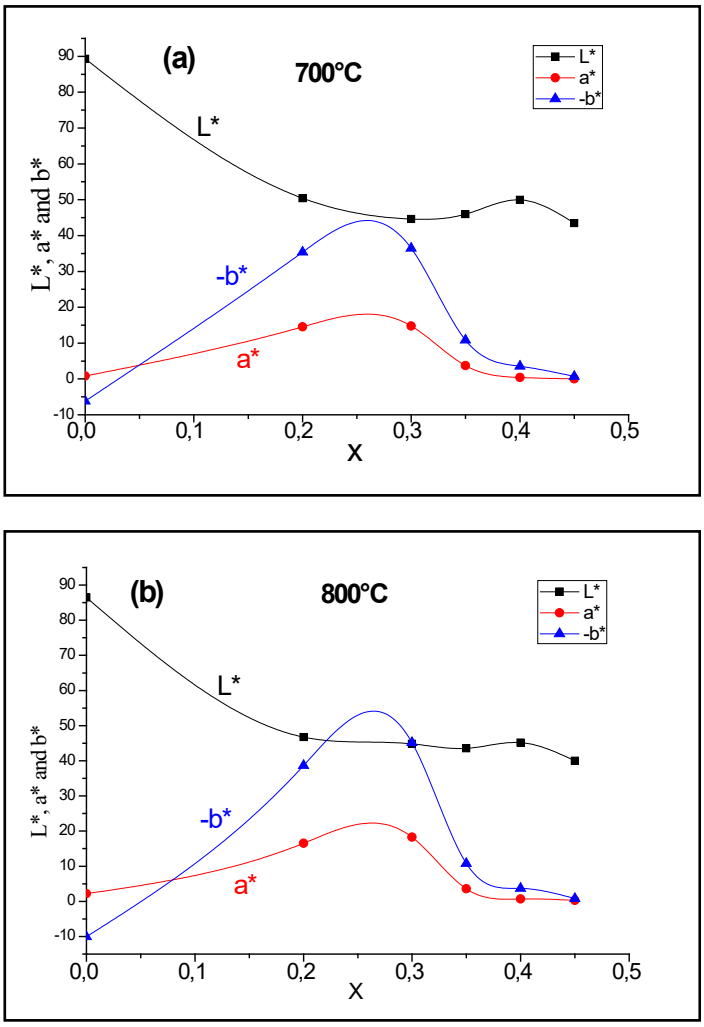

Fig. 15. Evolution of the colour parameters of $Zn_{1-x}Co_xMoO_4$ powders with ($0 \leq x \leq 0.45$) obtained by solid state reactions at (a) 700°C and (b) 800°C.

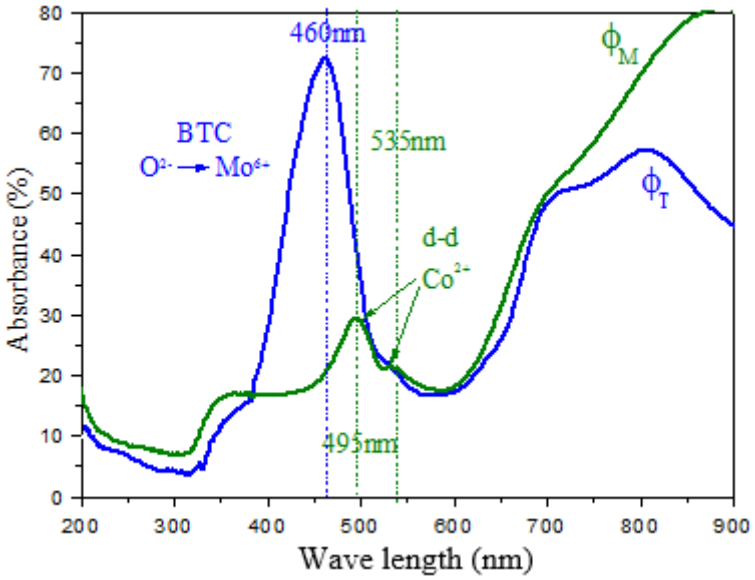

Fig. 16. UV-Vis absorption spectra of $Zn_{0.7}Co_{0.3}MoO_4$ (φ_T) and $Zn_{0.4}Co_{0.6}MoO_4$ (φ_M) obtained at 700°C.